SCIENCE CHINA
Information Sciences

• RESEARCH PAPER •

November 2017, Vol. 60 112301:1–112301:10
doi: 10.1007/s11432-016-9069-9

# Effect of orbital shadow at an Earth-Moon Lagrange point on relay communication mission

Yuhua TANG[1,2], Weiren WU[2], Dong QIAO[1,3*] & Xiangyu LI[1,3]

[1]*School of Aerospace Engineering, Beijing Institute of Technology, Beijing* 100081*, China;*
[2]*Center of Lunar Exploration and Aerospace Engineering, Beijing* 100037*, China;*
[3]*Key Laboratory of Autonomous Navigation and Control for Deep Space Exploration, Ministry of Industry and Information Technology, Beijing* 100081*, China*

Received November 16, 2016; accepted February 9, 2017; published online September 19, 2017

**Abstract** The shadow effect is an important constraint to be considered during the implementation of exploration missions. In this paper, for the Earth-Moon Lagrange point L2 relay communication mission, shadow effect issues on a periodic orbit about L2 are investigated. A systematic analysis based on the time domain and phase space is performed including the distribution, duration, and frequency of shadows. First, the Lindstedt-Poincare and second-order differential correction methods are used in conjunction with the DE421 planetary ephemeris to achieve a mission trajectory family in a high-precision ephemeris model. Next, on the basis of a conical shadow model, the influence of different orbital phases and amplitudes on the shadow is analyzed. The distribution of the shadow is investigated as well. Finally, the configuration of the shadow and its characteristics are studied. This study provides an important reference and basis for mission orbit design and shadow avoidance for relay satellites at an Earth-Moon Lagrange point.

**Keywords** Earth-Moon system, equilibrium point, relay orbit, shadow effect, motion control

**Citation** Tang Y H, Wu W R, Qiao D, et al. Effect of orbital shadow at an Earth-Moon Lagrange point on relay communication mission. Sci China Inf Sci, 2017, 60(11): 112301, doi: 10.1007/s11432-016-9069-9

## 1 Introduction

Chang'E-4 will perform the first landing, roaming, and exploration tasks on the far side of the Moon. During the mission, the lander and the rover, which will land on the lunar far side, will not be able to communicate directly with Earth because of the synchronous rotation of the Moon. Therefore, such communications need to be transmitted by a relay satellite. A periodic orbit about the Earth-Moon Lagrange point L2, owing to its unique dynamic characteristics, provides advantages, such as a relatively constant geometric relationship between the satellite and the Moon, long duration in Earth's field of view, and low-cost orbital maintenance. It is, therefore considered to be an ideal position for relay communication.

The concept of deploying relay satellites at the Earth-Moon L2 point was proposed in the 1970s [1]. Since then many studies concerning Earth-Moon low-energy transfer [2–4] and station keeping have been conducted [5–9]. In contrast, little research on illumination and shadow effects on satellites operating in

* Corresponding author (email: qiaodong@bit.edu.cn)

 

a periodic orbit of the Earth-Moon L2 point has been reported. As the angle between the Moon's orbital plane and the ecliptic plane varies over time, relay satellites in a periodic orbit about an equilibrium point will not be illuminated in certain periods owing to the shadow of the Earth or the Moon. The duration of these shadows plays an important role in the design of a relay satellite power supply system. Long-term shadows will result in insufficient power supply and consequently affect the success of relay tasks [10].

This paper is intended to address shadow effects on relay satellites in a halo orbit about the Earth-Moon L2 point. In particular, we focus on analyzing the duration and distribution of the shadow effect for different orbital phases and orbital amplitudes, on the basis of which suggestions for mission orbit design are proposed. Further, a systematic analysis of the configuration, frequency and duration of a single shadow is presented.

## 2 Relay satellite mission orbit in precise ephemeris models

### 2.1 Restricted three-body model, equilibrium point and periodic orbit

The circular restricted three-body problem (CRTBP) can be employed to describe the movement of a relay satellite in the Earth-Moon system. The dimensionless dynamic equations in the centroid rotation system can be written as follows:

$$\begin{cases} \ddot{x} - 2\dot{y} - x = -\dfrac{(1-\mu)(x+\mu)}{r_1^3} - \dfrac{\mu(x-1+\mu)}{r_2^3}, \\ \ddot{y} + 2\dot{x} - y = -\dfrac{(1-\mu)y}{r_1^3} - \dfrac{\mu y}{r_2^3}, \\ \ddot{z} = -\dfrac{(1-\mu)z}{r_1^3} - \dfrac{\mu z}{r_2^3}, \end{cases} \tag{1}$$

where $\mu$ is the system mass ratio. In the Earth-Moon system, $\mu = 0.01215$. In addition, $r_1, r_2$ are the distances from the satellite to the Earth and to the Moon respectively. $r_1 = \sqrt{(x+\mu)^2 + y^2 + z^2}$ and $r_2 = \sqrt{(x-1+\mu)^2 + y^2 + z^2}$. A normalized length, mass, and time are applied here, which are defined as the average Earth-Moon distance, system mass, and inverse of the Moon orbital angular speed respectively.

Five dynamic equilibrium points, i.e., Lagrange points, exist for the CRTBP: three collinear equilibrium points (L1, L2, and L3) and two triangular equilibrium points (L4 and L5). The L2 point, which can be used for relay communication is located on the opposite side of the Moon from the Earth.

According to the Lindstedt-Poincare method [11], the motion equation near the Earth-Moon L2 point can be written as

$$\begin{cases} \ddot{\xi} - 2\dot{\eta} - (1+2c_2)\xi = \dfrac{\partial}{\partial \xi} \displaystyle\sum_{n \geqslant 3} c_n(\mu)\rho^n P_n\left(\frac{\xi}{\rho}\right), \\ \ddot{\eta} + 2\dot{\xi} + (c_2 - 1)\eta = \dfrac{\partial}{\partial \eta} \displaystyle\sum_{n \geqslant 3} c_n(\mu)\rho^n P_n\left(\frac{\xi}{\rho}\right), \\ \ddot{\zeta} + c_2\zeta = \dfrac{\partial}{\partial \zeta} \displaystyle\sum_{n \geqslant 3} c_n(\mu)\rho^n P_n\left(\frac{\xi}{\rho}\right), \end{cases} \tag{2}$$

where $\rho^2 = x^2 + y^2 + z^2$, and $c_2(\mu), c_n(\mu)$ are functions of only the mass and can be expressed as

$$\begin{cases} c_2 = \dfrac{1}{\gamma^3}\left[\mu + (1-\mu)\dfrac{\gamma^3}{(1+\gamma)^3}\right], \\ c_n(\mu) = \dfrac{1}{\gamma^3}\left[(-1)^n\mu + (-1)^n(1-\mu)\left(\dfrac{\gamma}{1+\gamma}\right)^{n+1}\right], \quad n \geqslant 3, \end{cases} \tag{3}$$

where $\gamma$ is the distance between the L2 point and the Moon, and $p_n$ is the $n$th-order Legendre polynomial.

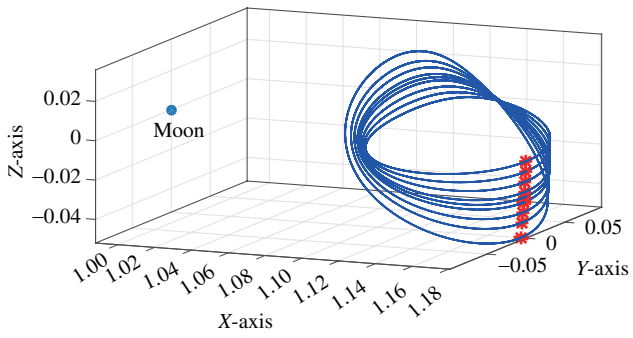


**Figure 1** (Color online) Southern family of halo orbit in the Earth-Moon three-body system.

The high-order approximate analytic solution of (2) can be expressed as

$$\begin{cases} \xi(t) = \sum\limits_{i,j}^{\infty} \left( \sum\limits_{|k|\leqslant i,|m|\leqslant j} \xi_{ijkm} \cos(k\theta_1 + m\theta_2) \right) \alpha^i \beta^j, \\ \eta(t) = \sum\limits_{i,j}^{\infty} \left( \sum\limits_{|k|\leqslant i,|m|\leqslant j} \eta_{ijkm} \sin(k\theta_1 + m\theta_2) \right) \alpha^i \beta^j, \\ \zeta(t) = \sum\limits_{i,j}^{\infty} \left( \sum\limits_{|k|\leqslant i,|m|\leqslant j} \zeta_{ijkm} \cos(k\theta_1 + m\theta_2) \right) \alpha^i \beta^j, \end{cases} \tag{4}$$

where $\alpha$ and $\beta$ represent the in-plane and out-of-plane amplitudes, respectively. $\theta_1 = \omega t + \phi_1$, and $\theta_2 = vt + \phi_2$. $\phi_1, \phi_2$ are initial phases. $\omega, v$ are power functions, that describe the orbital vibration amplitude:

$$\omega = \omega_p + \sum_{i,j}^{\infty} \omega_{ij} \alpha^i \beta^j, \quad v = \omega_v + \sum_{i,j}^{\infty} v_{ij} \alpha^i \beta^j. \tag{5}$$

The approximate analytic solution for a periodic orbit around the Earth-Moon L2 point can be obtained using (4). An accurate numerical solution can be obtained by the differential correction method. The southern family of halo orbits with different amplitudes around the L2 point in the Earth-Moon system obtained using the above process is shown in Figure 1.

For convenience, the phase angle $\theta$ of the halo orbit is defined as the angle between the projection of any orbital point on the $XY$-plane and the $X$ axis, and this angle has a positive value along the clockwise direction. The initial point of the phase angle $\theta$ is selected as the peak of the halo orbit on the negative $Y$ axis (as indicated by the marks in Figure 1).

### 2.2 Periodic orbit in a high-fidelity ephemeris model

To systematically analyze the shadow effect on relay satellites, the relative positions of the Sun, Earth, and Moon have to be considered. Therefore, a high-fidelity ephemeris model is employed in this study [12]. In this paper, we adopt the DE 421 planetary ephemeris.

Assume that the position vector of a relay satellite in the selenocentric inertial coordinate system is $[x_i, y_i, z_i]$, the velocity vector is $[\dot{x}_i, \dot{y}_i, \dot{z}_i]$, and the instantaneous angular velocity of the Earth-Moon rotation system relative to the inertial coordinate system is $[0, 0, \omega]$. According to the ephemeris, the relative position and speed of the Moon in the geocentric frame are obtained as

$$L = a(1 - e\cos(E)). \tag{6}$$

If we take the average Earth-Moon distance $D$ as the normalized unit length, the actual Earth-Moon distance can be expressed as $R = L/D$. Under the ephemeris model, the Earth's position in the Earth-Moon rotation system is $[R(1-\mu), 0, 0]$, and the instantaneous equilibrium point position is $R\lambda$, where

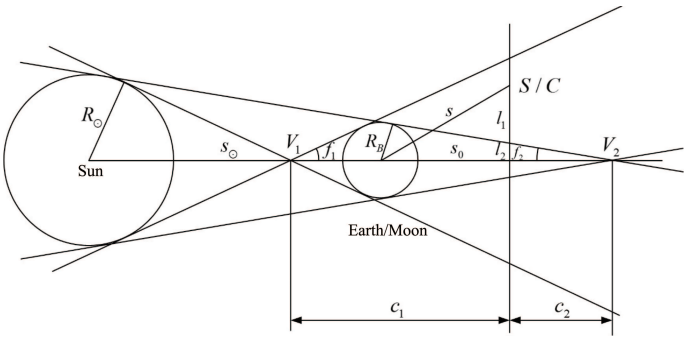


**Figure 2** Geometrical relations of the shadow effect.

$\lambda$ is the position of the equilibrium point in the CRTBP. The position of the satellite in the ephemeris rotational coordinate system can be expressed as

$$[x + R(1-\mu)\lambda, y, z]\,. \tag{7}$$

The position of the satellite relative to the Moon is

$$[x + R(1-\mu)\lambda - R(1-\mu), y, z]\,. \tag{8}$$

Then the position of the satellite relative to the Moon in the inertial coordinate system can be expressed as

$$\boldsymbol{r}_{i\mathrm{M}} = \begin{bmatrix} x_i \\ y_i \\ z_i \end{bmatrix} = DR_z(-\Omega)R_x(-i)R_z(-\varpi-\theta-\pi) \begin{bmatrix} x + (R-1)\lambda - R(1-\mu) \\ y \\ z \end{bmatrix}, \tag{9}$$

where $\Omega$, $i$, $\varpi$ and $\theta$ are the ascending node right ascension, orbit inclination, perigee argument, and true anomaly of the Moon relative to the Earth, respectively. $R_x$ and $R_z$ represent the rotational matrices around the $X$ and $Z$ axis, respectively. Similarly, the speed $\boldsymbol{v}_{i\mathrm{M}}$ relative to the Moon in the selenocentric inertial coordinate system can be obtained.

Using the ephemeris, the position $\boldsymbol{r}_{\mathrm{EM}}$ and speed $\boldsymbol{v}_{\mathrm{EM}}$ of the Moon relative to the Earth at any moment can be obtained. Therefore, the position and speed of the spacecraft relative to the Earth in the geocentric inertial coordinate system can then be expressed as

$$\begin{cases} \boldsymbol{r}_{i\mathrm{E}} = \boldsymbol{r}_{\mathrm{EM}} + \boldsymbol{r}_{i\mathrm{M}}, \\ \boldsymbol{v}_{i\mathrm{E}} = \boldsymbol{v}_{\mathrm{EM}} + \boldsymbol{v}_{i\mathrm{M}}. \end{cases} \tag{10}$$

## 3 Shadow model

A conical shadow model is used to describe the shadow effect of the Earth and Moon on relay satellites [13]. Here, the shadow factor $\nu$ is defined as

$$\nu = \frac{S}{S_\odot}, \tag{11}$$

where $S$ represents the visible Sun area, and $S_\odot$ is the total apparent area of the Sun. The geometrical relations of the shadow effect are shown in Figure 2.

$S_0 = \boldsymbol{L}\cdot\boldsymbol{R}$ is defined as the distance between the reference point and the Earth's center, where $\boldsymbol{L}$ is the unit vector from the Sun to the Earth, and $\boldsymbol{R}$ is the position vector of the relay satellite in the geocentric coordinate system. If $S_0 \leqslant 0$, the relay satellite lies on the sunward side, and there is no shadow: i.e., $\nu = 1$. If $S_0 > 0$, the geometrical relations should be used to determine whether the relay satellite will lie in the shadow zone.

First, the radius of the relay satellite on the reference plane is solved as $l_p = \sqrt{R^2 - S_0^2}$ , and the cone angle is calculated as

$$\begin{cases} \sin f_1 = (R_\odot + R_B)/S_\odot, \\ \sin f_2 = (R_\odot - R_B)/S_\odot, \end{cases} \tag{12}$$

where $R_\odot$ is the Sun's radius, $R_B$ is the Earth's radius, and $S_\odot$ is the distance between the Sun and the Earth. The critical distances $l_1, l_2$ are

$$\begin{cases} l_1 = c_1 \tan f_1, \\ l_2 = c_2 \tan f_2, \end{cases} \tag{13}$$

where $c_1, c_2$ are

$$\begin{cases} c_1 = \mathrm{S}_0 + R_B/\sin f_1, \\ c_2 = \mathrm{S}_0 - R_B/\sin f_2. \end{cases} \tag{14}$$

If $l_p < l_2$, and $\nu = 0$, the relay satellite lies in the complete shadow zone; if $l_2 \leqslant l_p < l_1$, and $0 < \nu < 1$, it lies in the half-shadow zone; if $l_1 \leqslant l_p$, and $\nu = 1$, it lies in the illuminated zone.

Because a relay satellite in a halo orbit may be obscured by both the Earth and the Moon, the Sun-Earth-satellite and Sun-Moon-satellite shadow models are established separately. In this paper, we do not distinguish the complete shadow zone and from the half shadow zone. Both of them are regarded as shadow zones.

## 4 Analysis of shadow effect on mission orbit

The mission orbit of a relay satellite is usually represented in the Earth-Moon rotational frame. The geometrical relations among the Sun, Earth, and Moon are time-dependent. The relative positions of these bodies are the key to shadow analysis. Thus, this study is based on a high-fidelity ephemeris model. A search method combining the time domain and phase space is developed to study the distribution of mission orbital shadows under different orbital phases and orbital amplitudes during the mission period. Finally, the shadow configuration is discussed and the evolution of different configurations on halo orbits is analyzed.

### 4.1 Shadow distribution for different orbital phases

Assuming that the period of the mission orbit cycle is $T_p$ and the flight time of the relay satellite in one period is $t_h$ ($0 \leqslant t_h \leqslant T_p$), the position of a satellite in a halo orbit at different flight time points can be obtained by orbit integration, and can be expressed in terms of the phase angle $\theta$. Once the time is determined, the shadow status of halo orbit can be obtained using the shadow model described above. Here we select the mission period from June 1, 2018 to June 1, 2021. Considering the constraints on fuel consumption, visibility and relay quality, the amplitude of the mission orbit is chosen as 12000 km. The entire orbit is divided into 360 time segments, and a 1 h sampling interval is adopted. The shadow distribution characteristics are analyzed by mapping orbital positions to the corresponding phase angles. The shadow distribution for different phase angles during the mission duration is shown in Figure 3.

The $X$ axis in Figure 3 represents the on-orbit flight time of the relay satellite (starting from June 1, 2018), and the $Y$ axis represents the possible phase angle of the relay satellite in the mission orbit. The shadow effects of the Earth and Moon are marked by dots and asterisks, respectively. Figure 3 shows that the shadows caused by the Earth and Moon consist of several independent zones in time-phase space. Each zone corresponds to a shadow event. The size of the zone indicates the duration and range of the shadow effect. Further, Figure 3 shows that the shadow caused by the Earth and Moon occur periodically with a certain frequency. The Moon's shadow appears every month and is distributed mainly in two areas, whereas the Earth's shadow appears less often (about every half year) but covers a larger area. The total shadow time for different phases of the mission orbit throughout the mission period is shown in Figure 4, and the shadow frequency is shown in Figure 5.

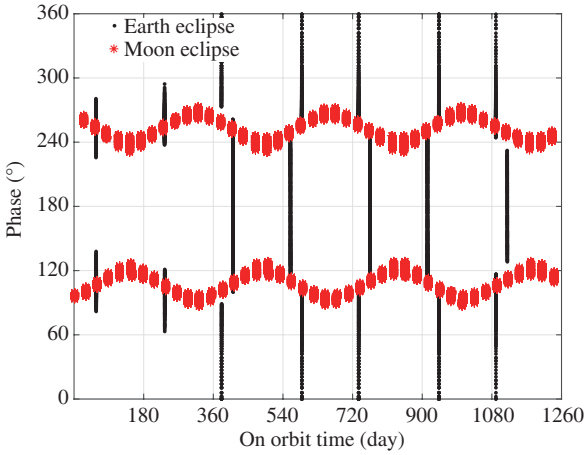


**Figure 3** (Color online) Distribution of orbital shadow in time-phase space.

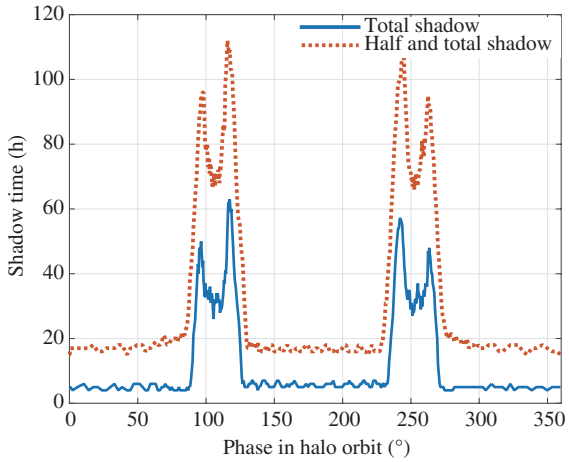


**Figure 4** (Color online) Distribution of total shadow time for different orbital phases.

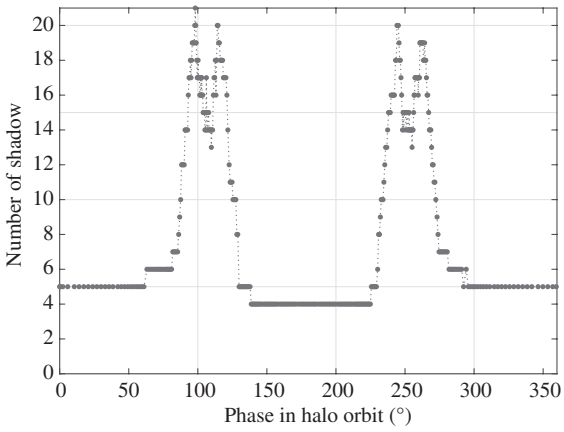


**Figure 5** Number of shadow events for different orbital phases.

**Table 1** Extreme values of orbital shadow duration and frequency

| Phase (°) | Shadow duration (h) | Phase (°) | Number of shadow |
|---|---|---|---|
| 96.72 | 97 | 98.19 | 21 |
| 115.6 | 112 | 114.4 | 21 |
| 244.2 | 111 | 244.2 | 20 |
| 262.5 | 96 | 264.4 | 19 |

In Figures 4 and 5, the $X$ axis represents the corresponding phase angle of the mission orbit, and $Y$-axis represents total shadow time and number of shadow events, respectively. Figures 4 and 5 show that during the mission period, all phases of the mission orbit will suffer from shadow, but with significant variation in duration and frequency. For phase angles in the ranges $[91°, 122°]$ and $[235°, 268°]$, the total shadow duration is about 100 h, and the maximum total shadow duration reaches 112 h, including 21 shadow events. Both the total shadow duration and the shadow frequency exhibit four apparent peaks. The extreme values are shown in Table 1.

The above discussion considers the shadow distribution in the phase space. In addition, if we further introduce the motion of the spacecraft, the shadow time for the spacecraft during the mission can be obtained. The initial states of a spacecraft in a halo orbit are defined in the phase space. Then the state of the spacecraft at an arbitrary time could be obtained according to its initial state and on orbit time. If the state of the spacecraft coincides with the shadow zone, the spacecraft will suffer from shadow.

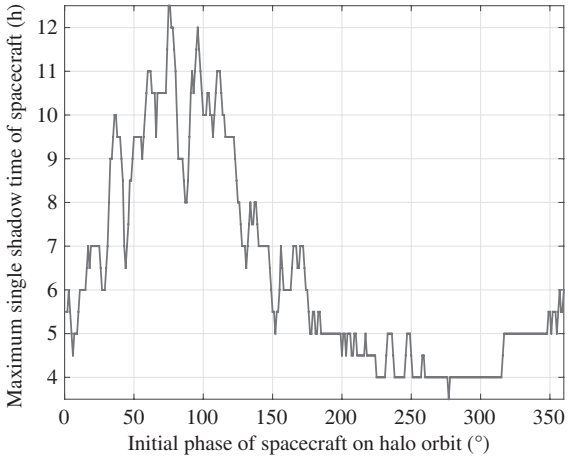


**Figure 6** Maximum single shadow time of spacecraft.

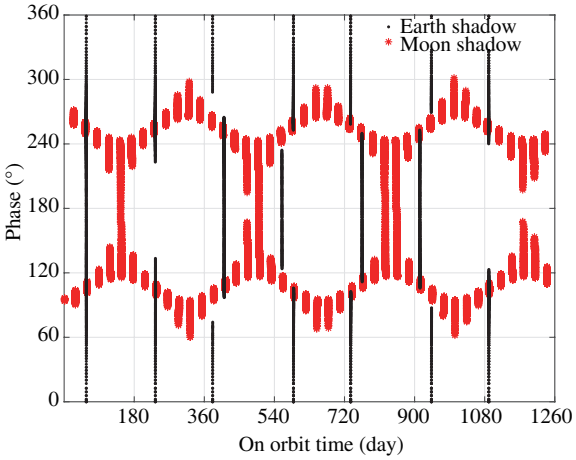


**Figure 7** (Color online) Distribution of orbital shadow for 9000 km amplitude.

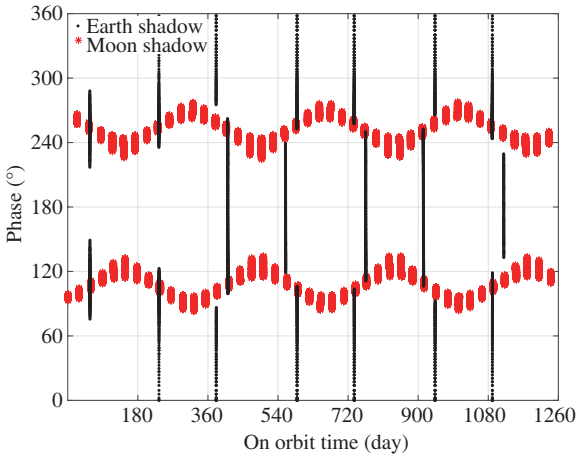


**Figure 8** (Color online) Distribution of orbital shadow for 11000 km amplitude.

The single shadow of duration of the spacecraft is a very important constraint on its power design. The maximum single shadow for different initial phases is analyzed, and the result is shown in Figure 6.

As shown in Figure 6, the maximum single shadow time varies from less than 4 h to more than 12 h for different initial phases of the spacecraft. The optimal initial phase of the spacecraft is between 260° and 313°.

### 4.2 Influence of mission orbital amplitude on shadow distribution

Amplitude is an important feature of the halo orbit. In an actual mission, owing to the sensitivity to the dynamic environment and the impact of measurement as well as control errors, the orbital amplitude may change with time. In this section, we focus on analyzing the impact of different amplitudes on the shadow distribution, with particular cases of 9000, 11000, 13000, and 15000 km. The results are shown in Figures 7–10, respectively.

Figures 7–10 show that the shadow distribution depends strongly on the orbital amplitude, especially that of the Moon shadow. As the amplitude decreases, the duration and coverage region of each shadow event increase. Two shadow zones may even overlap at a phase angle near 180° (as shown in Figure 7). In contrast, if the mission's orbital amplitude increases, the maximum total shadow duration on for a halo orbit gradually decreases, as shown in Table 2. However, neither increasing nor decreasing the mission's orbital amplitude will obviously change the shadow frequency.

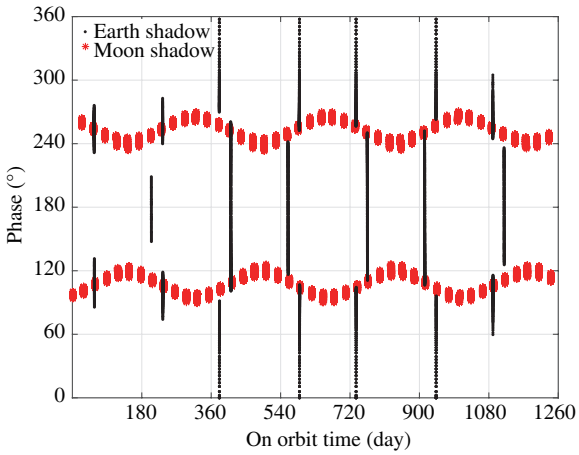


**Figure 9** (Color online) Distribution of orbital shadow for 13000 km amplitude.

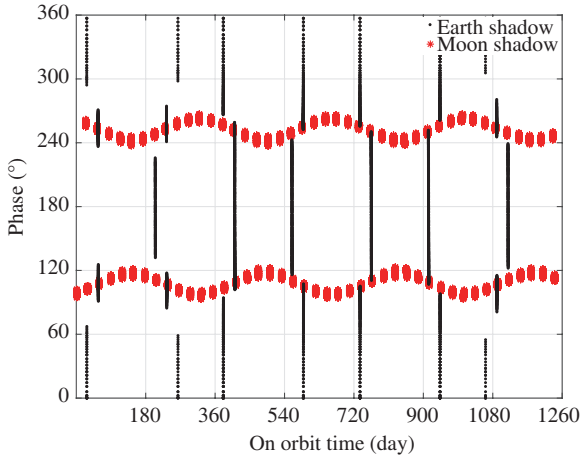


**Figure 10** (Color online) Distribution of orbital shadow for 15000 km amplitude.

**Table 2** Maximum shadow time of mission orbits and spacecraft for different orbital amplitudes

| Amplitude (km) | Maximum total shadow duration for orbits (h) | Maximum single shadow time for spacecraft (h) | |
|---|---|---|---|
| | | Upper bound | Lower bound |
| 9000 | 115 | 19.5 | 4.0 |
| 11000 | 113 | 14.0 | 3.5 |
| 12000 | 112 | 12.5 | 3.5 |
| 13000 | 110 | 11.5 | 3.5 |
| 15000 | 108 | 10.0 | 3.0 |

The change in the shadow distribution of a halo orbit will in turns change the duration of shadow on the spacecraft. The maximum single shadow for a spacecraft is also listed in Table 2. Both the upper and lower bounds of the shadow time decrease with increasing orbital amplitude. The longest duration of a single shadow decreases from 19.5 h for a 9000 km orbit to 10 h for a 15000 km orbit, which means that a larger-amplitude halo orbit is a more suitable mission orbit in terms of the shadow time.

### 4.3 Analysis of geometrical configuration of shadows

The geometrical configuration of shadows in the time domain and phase space reflects changes in the shadow zones over time, which are closely related to specific shadow effects on the relay satellite and the design of the shadow avoidance strategy. The analysis in this section focuses on the geometrical configuration of the shadow zones. Assuming a mission orbit with an amplitude of 12000 km, the shapes of the shadow zones in each shadow event are classified and compared, as shown in Figure 11.

Figure 11 shows that owing to the complicated geometrical relations among the Sun, Earth, and Moon, the geometrical configuration of each shadow event is different in the time domain and phase space. However, these configurations can be roughly classified into four groups, indicated by $a$, $b$, $c$, $d$ in the figure. Configuration $a$ has a crescent shape, with different slope directions at the upper and lower boundaries of the shadow zones. Configurations $b$ and $c$ both have a long narrow shape. The difference is that the upper and lower boundaries of configuration $b$ extend downward along the $X$ axis, whereas those of configuration $c$ are exactly the opposite. The upper and lower boundaries of configuration $d$ extend nearly parallel to the $X$ axis.

It is also discovered that the shadows caused by the Earth and Moon correspond to different shadow configurations. For an orbit with an amplitude of 12000 km, configuration $a$ exists only in the Earth shadow and appears only during the first year, whereas configuration $b$ appears periodically in the Moon shadow. The last two configurations appear in both the Earth and Moon shadows, though with different frequencies and phase ranges. Tables 3 and 4 show the frequency, distribution and maximum single

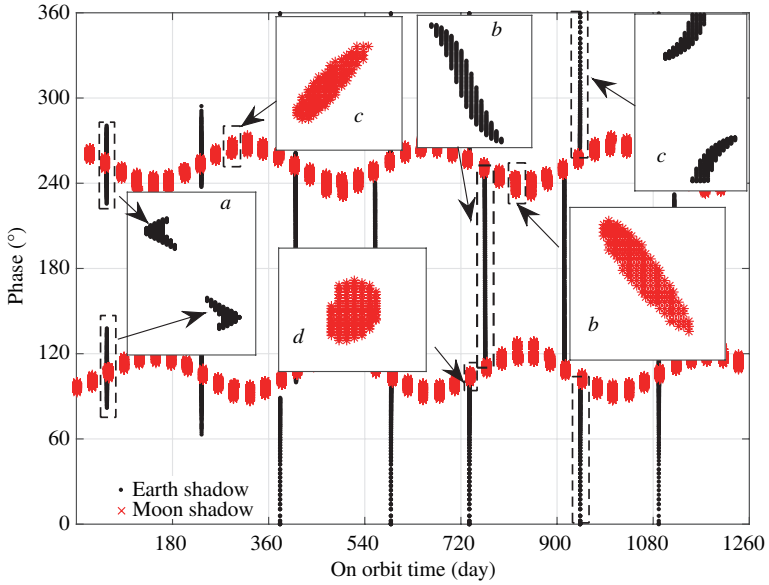


**Figure 11** (Color online) Different shadow configurations.

**Table 3** Distribution of shadow configurations in Earth shadow

| Configuration | Frequency | Range of phase (°) | Maximum single shadow time (h) |
|---|---|---|---|
| *a* | Twice (only in the first year) | 61–137 | 5.0 |
| | Twice (only in the first year) | 225–294 | |
| *b* | Every half year (the second and third years) | 110–261 | 4.0 |
| *c* | Every half year (the second and third years) | −116–116 | 5.5 |

**Table 4** Distribution of shadow configurations in Moon shadow

| Configuration | Frequency | Range of phase (°) | Maximum single shadow time (h) |
|---|---|---|---|
| *b* | Five times a year | 230–251 | 5.5 |
| | Five times a year | 107–127 | |
| *c* | Five times a year | 86–106 | 11.0 |
| | Five times a year | 254–273 | |
| *d* | Twice a year | 249–258 | 7.0 |
| | Twice a year | 101–112 | |

shadow time of the four shadow configurations in the Earth and Moon shadows, respectively.

The slope of the upper and lower boundaries of the four configurations reflects the evolution of the shadow on halo orbits. A positive slope indicates an increase in the coverage phase angle over time, and a negative one indicates a decrease in the phase angle over time. This study discovered that the shadow-covered phase in configuration *b* decreases over time, which means that shadow moves counterclockwise on halo orbits. In contrast, the shadow in configuration *c* moves clockwise on halo orbits. The phase in configuration *d* remains nearly unchanged over time, which means that the shadow remains relatively stationary on halo orbits. For configuration *a*, the shadow moves both counterclockwise and clockwise along the orbit. According to the dynamics of the CRTBP, the spacecraft always moves clockwise on halo orbits. Therefore, shadow configuration *c* has the same direction of motion as the spacecraft, which may cause a long-term shadow during the mission. The results in Tables 3 and 4 prove the confirm this deduction, as configuration *c* has the longest shadow time, whereas configuration *b* has the shortest shadow time. The mission design, therefore, should avoid configuration *c* as much as possible during the mission. These results could provide a reference for mission design and shadow avoidance.

## 5 Conclusion

The shadow effect on the mission orbit of relay satellites at the Earth-Moon L2 point are studied and analyzed on the basis of a high-precision ephemeris model and a conical shadow model. A search method combining the time domain and phase space is used to analyze the shadow distribution on the mission orbit for a three-year on-orbit period. In addition, the impact of different phase angles and amplitudes of the mission orbit on the shadow zone is discussed. The study shows that the Moon's shadow appears every month, and the phase angles are concentrated in two zones. The shadow caused by the Earth appears about every half year in the case of large coverage. Further, increasing the orbital amplitude will effectively decrease the duration of a single shadow. Finally, four types of geometrical shadow configurations are identified and the evolution of the shadow configurations on halo orbits is discussed. This study can provide a reference for the design of relay satellite mission orbits at the Earth-Moon L2 point and for strategic development in shadow avoidance.

**Acknowledgements** This work was supported by National Science and Technology Major Project of the Ministry of Science and Technology of China (Lunar Exploration Program), National Natural Science Foundation of China (Grant No. 11572038), and Chang Jiang Scholars Program.

**Conflict of interest** The authors declare that they have no conflict of interest.

## References

1 Farquhar R W. Lunar communications with libration-point satellites. J Spacecraft Rockets, 1967, 4: 1383–1384
2 Xu M, Xu S J. Trajectory and correction maneuver during the transfer from Earth to halo orbit. Chin J Aeronaut, 2008, 21: 200–206
3 Li M T, Zheng J H. Impulsive lunar halo transfers using the stable manifolds and lunar flybys. Acta Astronaut, 2010, 66: 1481–1492
4 Canalias E, Masdemont J J. Computing natural transfers between Sun C Earth and Earth C Moon lissajous libration point orbits. Acta Astronaut, 2008, 63: 238–248
5 Parker J S. Families of low-energy lunar halo transfers. In: Proceedings of AAS/AIAA Spaceflight Dynamics Conference, Tampa, 2006. 06-132
6 Kulkami J, Campbell M. Asymptotic stabilization of motion about an unstable orbit: application to spacecraft flight in halo orbit. In: Proceeding of the 2004 American Control Conference, Boston, 2004. 1025–1030
7 Xu M, Zhou N, Wang J L. Robust adaptive strategy for station keeping of halo orbit. In: Proceedings of the 24th Chinese Control and Decision Conference, Taiyuan, 2012. 3086–3091
8 Keeter T M. Station-keeping strategies for libration point orbit: target point and floquet mode approaches. Dissertation for Master's Degree. Indiana: Purdue University, West Lafayette, 1994. 145–148
9 Liu L, Cao J F, Hu S J, et al. Maintenance of relay orbit about the Earth-Moon collinear libration points. J Deep Space Explor, 2015, 2: 318–324
10 Dong G L, Xu D Z, Li H T, et al. Initial result of the Chinese Deep Space Stations' coordinates from Chinese domestic VLBI experiments. Sci China Inf Sci, 2017, 60: 012203
11 Jorba A, Masdemond J. Dynamics in the centre manifold of the collinear points of the restricted three body problem. Phys D, 1999, 132: 189–213
12 Li M T. Low energy trajectory design and optimization for collinear libration points missions. Dissertation for Ph.D. Degree. Beijing: Center for Space Science and Applied Research Chinese Academy of Sciences, 2010. 46–49
13 Montenbruck O, Gill E. Satellite Orbits: Models, Methods and Application. 2nd ed. Berlin: Springer, 2001. 80–81